

# Emergent E-I Structure in Performance-Evolved Reservoir Networks of Neuronal Population Dynamics

Manish Yadav<sup>1</sup>

Chair of Cyber-Physical Systems in Mechanical Engineering, Technische Universität Berlin, Straße des 17. Juni 135, 10623 Berlin, Germany

(\*Electronic mail: manish.yadav@tu-berlin.de)

(Dated: 17 March 2026)

Understanding how network structure gives rise to neuronal dynamics and whether compact computational models can recover that structure from data alone is a central challenge in computational neuroscience. We apply the performance-dependent network evolution (PDNE) framework to model the dynamics of the Wilson-Cowan (WC) neuronal system, a canonical two-population model of excitatory-inhibitory (E-I) interaction underlying physiological rhythms. Starting from a minimal seed network, PDNE iteratively grows and prunes a reservoir computing (RC) network based solely on prediction performance, yielding compact, task-optimized reservoir networks. The evolved networks accurately predict both excitatory  $E(t)$  and inhibitory  $I(t)$  population activities across unseen stimulus amplitudes and generalize in a zero-shot manner to novel stimulus configurations: varying pulse number, position and amplitude without retraining. Structural analysis of the evolved networks reveals a consistent functional organization with nodes specialized for E, I, and shared E-I representations. Importantly, the population-level connectivity of the evolved reservoirs spontaneously recovers the correct excitatory-inhibitory sign pattern of the WC model for three of four interaction types, without this being imposed by design. These results demonstrate that performance-driven network evolution can produce not only accurate but structurally interpretable models of physiological rhythms, opening a path toward compact, data-efficient digital twins of neuronal systems.

## I. INTRODUCTION

The brain is a paradigmatic example of a complex physiological network whose emergent rhythms from slow delta oscillations to fast gamma bursts, arising from the interplay of excitatory and inhibitory neuronal populations<sup>1,2</sup>. Understanding how network structure gives rise to these dynamics, and conversely, how dynamical function constrains network topology, is a central challenge in computational neuroscience and brain-inspired computing<sup>3</sup>. Recent advances in machine learning have opened new avenues for data-driven modeling of such physiological rhythms, yet dominant deep learning frameworks remain largely black-box systems: they predict well but offer little insight into the mechanisms underlying the dynamics they approximate<sup>4</sup>. This tension between predictive power and interpretability motivates the search for smaller, more structured, and mechanistically transparent computational models.

Neuronal population models, such as the Wilson-Cowan (WC) model<sup>5</sup>, capture the essential dynamics of excitatory-inhibitory (E-I) interactions with minimal parameterization, producing rich dynamical repertoires including fixed points, limit cycles, and bistability. Reproducing such dynamics with machine learning models has been attempted with recurrent neural networks and neural ordinary differential equations<sup>6,7</sup>, but these approaches typically require large numbers of parameters and provide limited structural interpretability. A key open question is whether a compact, learnable dynamical system can not only predict neuronal population activity across varying stimulus conditions, but also develop an internal structure that reflects the underlying E-I organization of the target system.

Reservoir computing (RC)<sup>8,9</sup> offers a promising framework

in this direction. Grounded in dynamical systems theory, RC exploits the rich transient dynamics of a fixed recurrent network, the reservoir, to project input signals into a high-dimensional state space, from which outputs are read out via simple linear regression (Fig. 1 (a)). This separation of dynamics and learning makes RC both computationally efficient and analytically tractable. For discrete-time systems, the reservoir state evolves as:

$$\mathbf{r}_{t+1} = (1 - \alpha)\mathbf{r}_t + \alpha G(\mathbf{A}\mathbf{r}_t + \mathbf{W}_{\text{in}}\mathbf{u}_t) \quad (1)$$

where  $\mathbf{r}_t$  is the reservoir state,  $\mathbf{u}_t$  the external input,  $\mathbf{A}$  the recurrent adjacency matrix,  $G$  a nonlinear activation function, and  $\alpha \in (0, 1]$  the leak rate. Only the linear readout weights  $\mathbf{W}_{\text{out}}$  are trained, making the approach highly efficient. However, the reservoir topology, typically random and fixed, which remains opaque, as there is no guarantee that its structure bears any relation to the dynamical system it is modeling. This raises a fundamental limitation: while RC can approximate complex dynamics, the *structure-function* relationship of the reservoir remains uninformative by construction. Increasing reservoir size does not reliably improve performance<sup>14</sup> and can introduce chaotic dynamics or signal degradation<sup>10,11</sup>. Systematic strategies for building smaller, task-optimized reservoirs are therefore essential, both for computational efficiency and for the prospect of structural interpretability<sup>12,13</sup>.

A step toward this goal was taken by Yadav et al.<sup>14</sup>, who introduced the performance-dependent network evolution (PDNE) framework: a biologically inspired mechanism that grows a reservoir from a minimal seed network by iteratively adding and pruning nodes based on prediction performance. Rather than fixing the topology before training, PDNE evolves the network structure alongside its function, yielding compact reservoirs adapted to the complexity of the

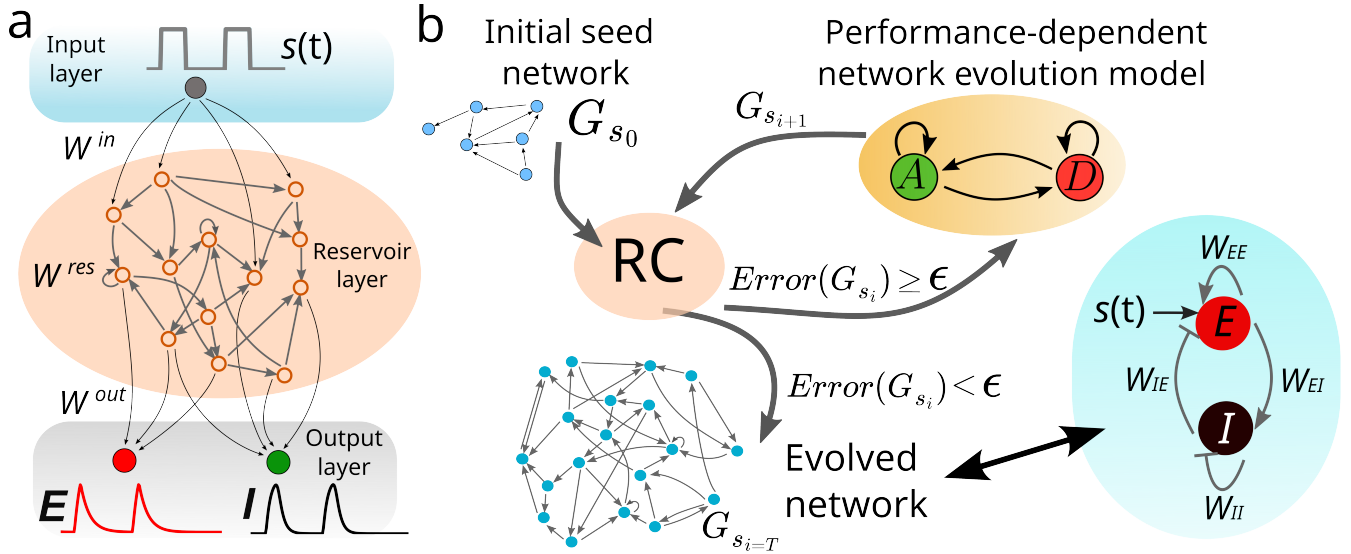


FIG. 1. **Performance-dependent network evolution for learning Wilson-Cowan neuronal dynamics.** (a) The reservoir computing (RC) model with input layer receiving pulse stimulus  $s(t)$ , recurrent reservoir layer  $W^{\text{res}}$ , and output layer predicting excitatory ( $E$ , red) and inhibitory ( $I$ , green) population activities. (b) The PDNE algorithm iteratively evolves the reservoir via node addition ( $A$ ) and deletion ( $D$ ) modules driven by prediction performance, from a minimal seed network  $G_{s_0}$  toward a task-optimized topology. Right: the target WC model with coupling weights  $W_{EE}$ ,  $W_{EI}$ ,  $W_{IE}$ , and  $W_{II}$ .

target task. Related ideas have been explored in deep neural networks through progressive growth strategies<sup>15</sup> and structured pruning<sup>16</sup>, demonstrating that performance-driven structural adaptation can improve both efficiency and generalization. Crucially, networks evolved under task-specific pressure may develop structural motifs that are not arbitrary but functionally meaningful, opening a path toward interpretable, structure-aware dynamical models.

In this work, we apply the PDNE framework to model the dynamics of the Wilson-Cowan neuronal system, a canonical model of E-I population dynamics underlying physiological rhythms. The WC model describes the mean activities of an excitatory population  $E(t)$  and an inhibitory population  $I(t)$  as:

$$\tau_E \frac{dE}{dt} = -E + S_E(w_{EE}E - w_{EI}I + s(t)) \quad (2)$$

$$\tau_I \frac{dI}{dt} = -I + S_I(w_{IE}E - w_{II}I) \quad (3)$$

where  $S_X$  is a sigmoidal activation function:

$$S_X(x) = \frac{1}{1 + \exp[-a_X(x - \theta_X)]}, \quad X \in \{E, I\} \quad (4)$$

and  $s(t)$  is an external pulse stimulus acting as the bifurcation parameter. Despite its simplicity, just two coupled equations of the WC model exhibits a rich dynamical repertoire, including monostability, bistability, and sustained oscillations, making it an ideal testbed for structure-aware dynamical modeling. All model parameters are provided in Appendix A.

Our central hypothesis is two-fold. First, that PDNE-evolved reservoirs can accurately predict WC population dy-

namics across unseen stimulus amplitudes and stimulus configurations, generalizing across the system's bifurcation landscape with far fewer parameters than standard large reservoirs. Second, and more fundamentally, that the topology of the evolved network will spontaneously reflect the E-I connectivity structure of the WC system is not by design, but as an emergent consequence of performance-driven structural adaptation. If realized, this would demonstrate that task-optimized network evolution can produce not just accurate but structurally interpretable models of physiological rhythms, where the learned network architecture encodes mechanistic information about the target system.

## II. METHODS: RC IMPLEMENTATION AND PDNE

### A. Reservoir Computing Implementation

Building on the RC framework of Eq. (1), here we specify the implementation used for modeling WC dynamics. The activation function is  $G = \tanh$ , the recurrent matrix  $W^{\text{res}} \in \mathbb{R}^{N \times N}$  is rescaled to spectral radius  $\rho$ , and a node-wise gain or scaling vector  $\mathbf{g} \in \mathbb{R}^N$  introduces heterogeneous activation sensitivities across nodes. Input weights  $W^{\text{in}} \in \mathbb{R}^N$  are nonzero only at designated input nodes  $\mathcal{I} \subseteq \{1, \dots, N\}$ . The predicted outputs are computed as linear readouts from designated output node subsets  $\mathcal{O}_i \subseteq \{1, \dots, N\}$  for each channel  $i \in \{E, I\}$ :

$$\hat{y}_i(t) = W_i^{\text{out}} \mathbf{r}_{\mathcal{O}_i}(t) \quad (5)$$

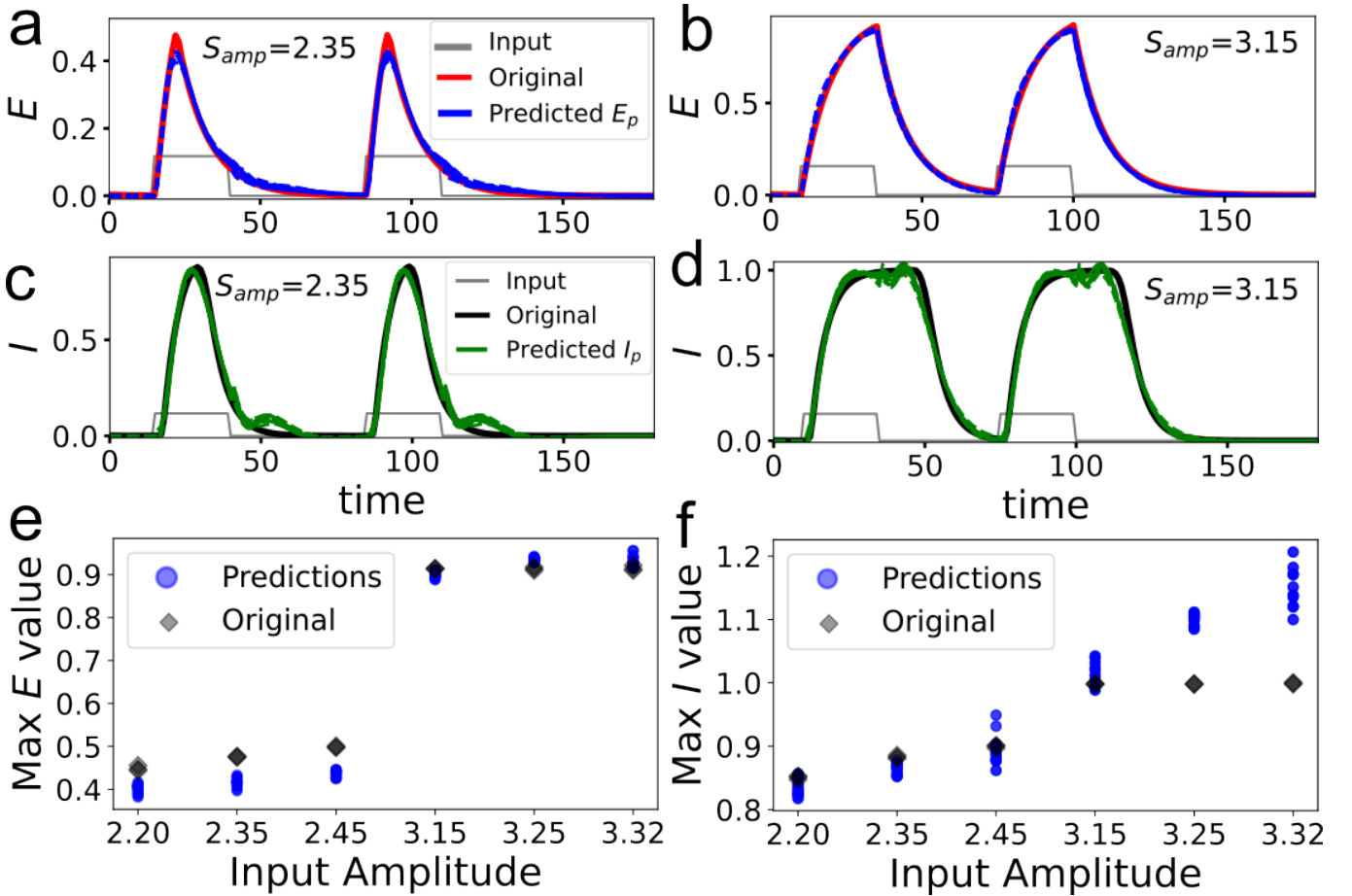


FIG. 2. **Prediction performance on unseen test stimuli.** *Top two rows:* Predictions of excitatory  $E(t)$  (red: original, blue:  $E_p$ ) and inhibitory  $I(t)$  (black: original, green:  $I_p$ ) for test amplitudes  $S_{amp} = 2.35$  (left) and  $S_{amp} = 3.15$  (right), both absent from the training set. *Bottom row:* Peak amplitude predictions (blue circles) vs. original peak values (gray diamonds) across 10 model repetitions. Arrows indicate systematic over- or under-estimation where present. The pulse input  $s(t)$  is scaled by  $1/20$  for visualization.

Output weights are obtained via ridge regression over all training batches simultaneously:

$$W_i^{\text{out}} = V_i R_{\theta_i}^{\top} (R_{\theta_i} R_{\theta_i}^{\top} + \beta \mathbf{I})^{-1} \quad (6)$$

where  $R_{\theta_i} \in \mathbb{R}^{|\theta_i| \times BT}$  is the matrix of reservoir states at output nodes concatenated across all  $B$  training batches and  $T$  timesteps,  $V_i$  the corresponding target output matrix, and  $\beta$  the regularization parameter.

## B. Performance-Dependent Network Evolution

Standard RC fixes the reservoir topology before training, limiting adaptability to the complexity of the target dynamics. We adopt the PDNE framework<sup>14</sup>, in which the reservoir topology is grown iteratively until a target prediction error is achieved. Starting from a minimal seed network of  $N_0$  nodes, the algorithm alternates between two structural operations, node addition and deletion (Fig. 1b) at each evolutionary step  $t$ :

*a. Node Addition (A).* A candidate node is proposed with  $k \sim \mathcal{U}\{1, k_{\max}\}$  random directed connections to existing nodes, with weights  $w \sim \mathcal{U}(-1, 1)$  and connection direction governed by probability  $\Psi$ . A node-wise gain  $g \sim \mathcal{U}(0.01, 1.0)$  is assigned. The candidate is added to input set  $\mathcal{I}$  with probability  $P_{\text{inp}}$  and independently to each output set  $\theta_i$  with probability  $P_{\text{out}}$ . Addition is accepted if the test NMSE strictly decreases across all channels  $\epsilon_{\text{new}}^{\text{pred}} < \epsilon_{\text{old}}^{\text{pred}}$  otherwise a new candidate is drawn, up to  $T_{\text{add}}$  attempts.

*b. Node Deletion (D).* Once any output channel satisfies  $\text{NMSE} < \Delta_{\epsilon}$ , a pruning phase is triggered. Up to  $\lfloor \rho_{\text{del}} N / 100 \rfloor$  deletion attempts are made, each randomly selecting a node for removal. Node indices are remapped after each deletion to maintain contiguous indexing. Deletion is accepted if the test NMSE does not increase on any channel  $\epsilon_{\text{new}}^{\text{pred}} \leq \epsilon_{\text{old}}^{\text{pred}}$  yielding a compact network retaining only task-relevant nodes. Evolution terminates when all channels satisfy  $\epsilon^{\text{pred}} \leq \Delta_{\epsilon}$  or the maximum evolution steps  $T$  is reached. The NMSE for output channel  $i$  is:

$$\epsilon_i = \frac{\sum_t (\hat{y}_i(t) - y_i(t))^2}{\sum_t (y_i(t) - \bar{y}_i)^2} \quad (7)$$

Performance is evaluated as the mean NMSE across  $B$  training amplitudes and  $N_{RC}$  independent RC initializations per evolution step to reduce stochastic variability.

### C. Training Data

We simulate the WC system under pulse stimuli of fixed duration  $T_{\text{pulse}}$  and varying amplitude. Training amplitudes  $\mathcal{A}_{\text{train}} = \{1.25, 1.5, 2.0, 2.5, 3.0\}$  span the excitable and oscillatory regimes, while test amplitudes  $\mathcal{A}_{\text{test}} = \{0.85, 1.4, 1.75, 2.25, 2.75\}$  are interleaved between training values to probe interpolation generalization. Each simulation is subsampled by a factor of 10 to obtain RC input-output sequences. All hyperparameters are summarized in Appendix A.

## III. PREDICTION PERFORMANCE AND GENERALIZATION

### A. Generalization Across Stimulus Amplitudes

A key requirement for a faithful model of the WC system is the ability to generalize beyond the training distribution, predicting population dynamics for stimulus amplitudes not seen during evolution. Fig. 2 shows predictions of the final evolved reservoir on two test amplitudes,  $S_{\text{amp}} = 2.35$  and  $S_{\text{amp}} = 3.15$ , both interleaved between training values and withheld throughout the PDNE procedure. In this open-loop setting, only the external pulse stimulus  $s(t)$  drives the reservoir at each timestep; predicted outputs  $\hat{E}(t)$  and  $\hat{I}(t)$  are computed purely from the evolved reservoir state without any feedback, making accurate prediction contingent entirely on the internalized dynamics of the evolved topology.

The top rows of Fig. 2 show that the evolved network accurately reproduces both population responses, capturing the transient peak, characteristic decay timescale, and return to baseline under both stimulus conditions. The inhibitory predictions closely track  $I(t)$  across both amplitudes, including the faster rise and sharper peak relative to  $E(t)$ , a direct consequence of the shorter inhibitory timescale  $\tau_I < \tau_E$  in the WC model. The excitatory predictions show slightly larger deviations near the peak at  $S_{\text{amp}} = 3.15$ , consistent with increased response nonlinearity at higher stimulus amplitudes.

The bottom row provides a quantitative assessment of peak amplitude prediction across 10 independent model repetitions. For  $S_{\text{amp}} = 2.35$ , predictions cluster tightly around the original peak values, indicating consistent generalization. For  $S_{\text{amp}} = 3.15$ , greater spread is observed, reflecting the increased variability of stochastic network evolution at higher response amplitudes. Notably, the reservoir reproduces  $I(t)$  accurately without ever receiving  $I$  as an input, relying solely on  $s(t)$ , suggesting that E-I coupling dynamics have been implicitly encoded in the evolved topology, a point examined structurally in Section IV.

### B. Zero-Shot Generalization to Novel Stimulus Configurations

A more stringent test of whether a learned model has internalized the underlying system dynamics rather than memorizing stimulus-response mappings, is its ability to generalize to structurally different inputs without retraining. Fig. 3 presents such a test: the PDNE-evolved reservoirs, trained exclusively on two-pulse sequences, are evaluated on entirely novel configurations varying in number of pulses, temporal positions, and amplitudes, with no retraining or fine-tuning.

Fig.3(a,b) panels show predictions for a single-pulse stimulus at  $S_{\text{amp}} = 2.35$  and  $3.25$  configurations structurally simpler than the training sequences confirming that the model does not require multiple pulses to produce accurate responses. Panels (c-l) demonstrate predictions across two- and three-pulse configurations spanning a range of amplitudes and temporal arrangements. The evolved reservoir accurately tracks both  $E(t)$  and  $I(t)$  across all configurations, correctly reproducing the response to each individual pulse, the amplitude scaling with stimulus strength, and the recovery dynamics between successive pulses.

This result carries an important implication: the reservoir has not learned a fixed input-output map tied to the specific two-pulse training format, but has instead internalized the reactive dynamics of the WC system, its ability to respond to an arbitrary pulse at any point in time with the correct excitatory and inhibitory trajectory. Each pulse effectively resets the system into a transient response, and the evolved network reproduces this reset-and-respond behavior across varying inter-pulse intervals and amplitudes. These findings demonstrate that PDNE-evolved reservoirs develop a generalizable internal model of WC dynamics, rather than a stimulus-specific approximation.

## IV. NETWORK EVOLUTION AND STRUCTURAL ANALYSIS

We next analyze how the network structure evolves while solving the WC modeling task, tracking prediction error, network size, connection density, and internal parameter distributions jointly as the reservoir grows and is pruned.

### A. Evolution Dynamics

Fig. 4 characterizes these dynamics across 10 independent model repetitions. Panels (a) and (b) show the training NMSE for the excitatory ( $\varepsilon_E$ ) and inhibitory ( $\varepsilon_I$ ) channels as a function of evolution step  $t$ . All repetitions begin from the same minimal seed (orange markers) and converge toward  $\Delta_\varepsilon$  (blue markers) via qualitatively consistent but stochastically distinct trajectories. The rapid initial error reduction reflects the high marginal utility of early node additions, while convergence slows as the network approaches the target threshold.

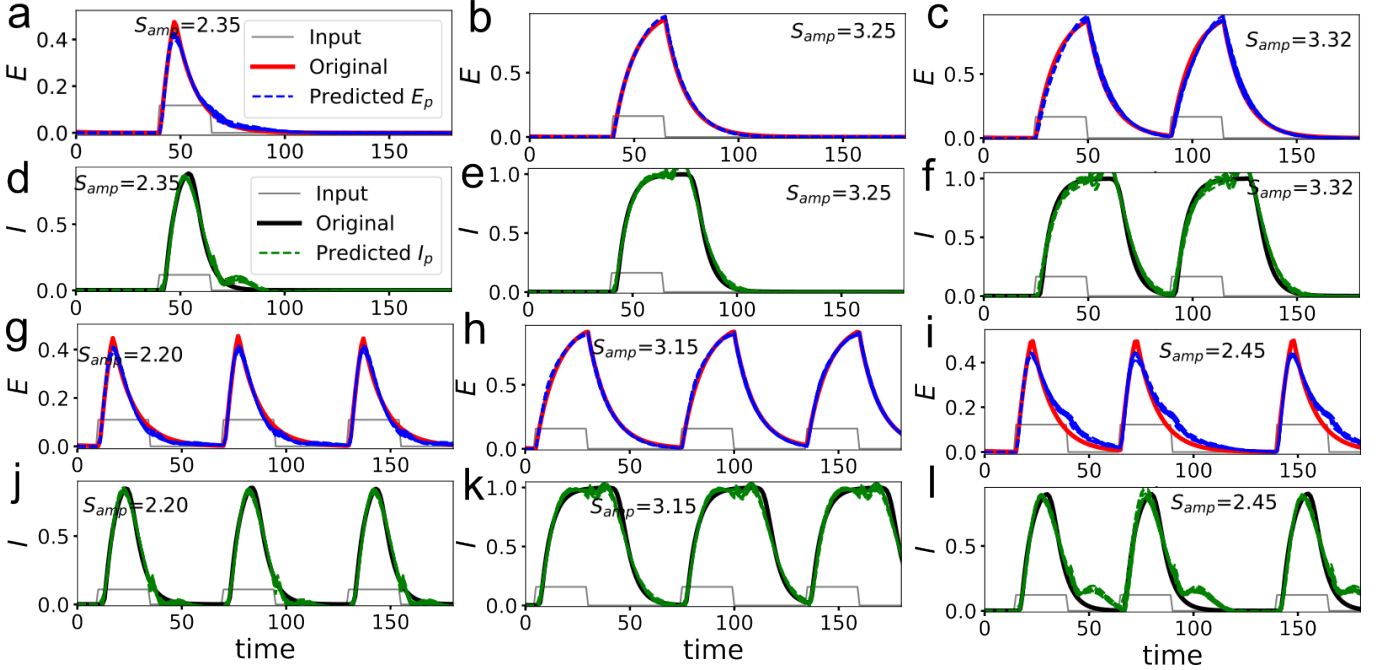


FIG. 3. **Zero-shot generalization to novel stimulus configurations.** Models trained exclusively on two-pulse sequences are tested on stimuli with varying number of pulses, positions, and amplitudes without retraining. Each panel pair shows  $E(t)$  (top: red original, blue dashed  $E_p$ ) and  $I(t)$  (bottom: black original, green dashed  $I_p$ ). (a,b) Single-pulse reference at  $S_{amp} = 2.35$  and  $3.25$ . (c-l) Multi-pulse stimuli at  $S_{amp} = 2.20, 2.45, 3.15, 3.25, 3.32$  with varying pulse counts and temporal positions. The pulse input  $s(t)$  is scaled by  $1/20$  for visualization.

The number of reservoir nodes  $N(t)$  are shown in fig.4 (c), whose sawtooth-like trajectory reflects the interplay of addition and deletion:  $N(t)$  grows as new nodes reduce prediction error, then decreases as redundant nodes are pruned. Final network sizes vary across repetitions ( $\bar{N} = 66 \pm 17$  nodes), reflecting the existence of multiple compact configurations capable of achieving the target performance. Panel (d) shows the joint evolution trajectory in the density-node parametric space. Starting from a dense but minimal seed, the network expands while density decreases as nodes are added faster than connections, before settling into a consistent region across repetitions. This convergence suggests the PDNE algorithm discovers a task-specific structural regime rather than growing the network arbitrarily.

The representative initial and final network topologies are shown in Fig.4 (e, f). The sparse seed network develops into a substantially richer recurrent structure with broader connectivity and a greater proportion of output nodes. Edge colors reveal the spontaneous emergence of both excitatory and inhibitory connections in the evolved network. This structural reorganization is quantified in panels (g) and (h). The node gain distribution broadens substantially after evolution from a narrow initial range to nearly the full admissible interval, introducing heterogeneous activation sensitivities that enrich reservoir dynamics. Correspondingly, the edge weight distribution restructures from one dominated by weak positive connections to a broad, near-symmetric distribution spanning both positive and negative values. The increased prevalence of negative weights corresponding to inhibitory interactions,

is consistent with the E-I coupling structure of the target WC system, suggesting that performance-driven evolution sculpts the reservoir topology toward dynamical motifs reflecting the functional organization of the underlying neuronal model.

## B. Functional Node Organization

We next carried out the structural analysis of the evolved reservoirs, examining whether the network topology reflects the E-I organization of the target WC system. We classify each reservoir node into four functional categories based on its readout weight contributions: E-specific (contributing primarily to  $\hat{E}$ ), I-specific (contributing primarily to  $\hat{I}$ ), Shared (contributing significantly to both), and Peripheral (contributing weakly to neither).

As shown in Fig. 5 (a, b), the node classification counts and percentage composition across 10 repetitions. Despite substantial variation in final network size ( $\bar{N} = 66 \pm 17$ ), the functional composition remains remarkably consistent: E-specific, I-specific, and Shared nodes account for approximately 19%, 23%, and 20% of the network respectively, with means of  $\bar{n}_E = 12.2 \pm 4.2$ ,  $\bar{n}_I = 14.9 \pm 4.5$ , and  $\bar{n}_S = 13.9 \pm 6.3$  nodes. The slight dominance of I-specific nodes is consistent with the faster inhibitory timescale  $\tau_I < \tau_E$  in the WC model, which places greater representational demands on the inhibitory population. The large proportion of Shared nodes are comparable in count to either specialized population, reflects the tight mutual E-I coupling in the WC system, requiring nodes that in-

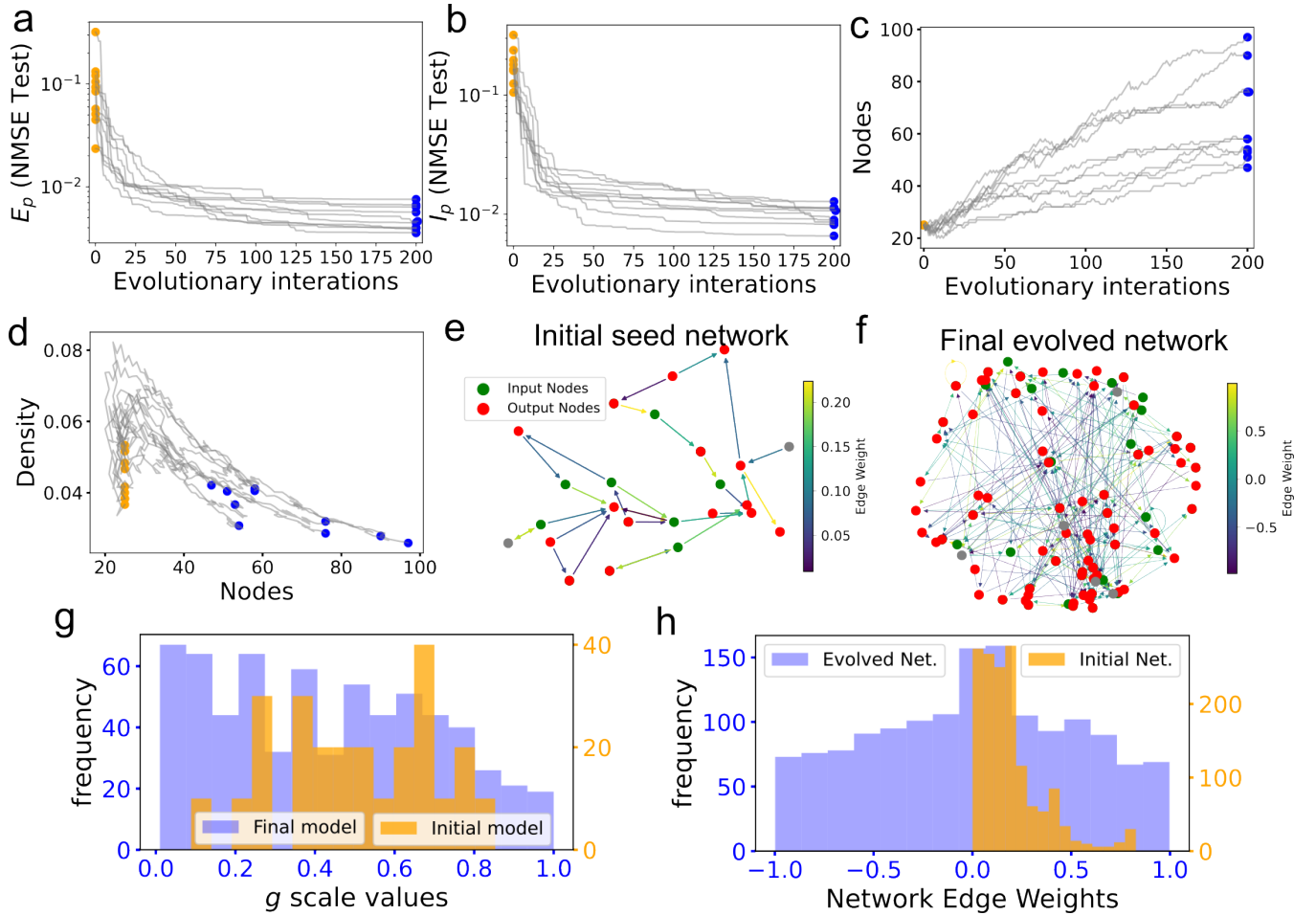


FIG. 4. **PDNE evolution dynamics and network topology across 10 model repetitions.** (a,b) Training NMSE for  $\epsilon_E$  and  $\epsilon_I$  vs. evolution step  $t$ . Orange: initial seed; blue: final evolved network. (c) Reservoir node count  $N(t)$  reflecting iterative addition and deletion. (d) Evolution trajectory in the density-node parametric space. (e,f) Representative initial and final network topologies. Green: input nodes  $\mathcal{I}$ ; red: output nodes  $\mathcal{O}_{E,I}$ ; gray: hidden nodes. Edge colors: connection weight (colorbar). (g,h) Distributions of node gain values  $g$  and edge weights for initial (orange) and evolved (blue) networks.

tegrate information from both populations. A representative evolved network topology colored by functional role is provided in Fig. 5(c). E-specific and I-specific nodes are spatially interleaved rather than segregated into distinct clusters, consistent with the distributed solution discovered by the PDNE algorithm.

### C. Structural Correspondence with Wilson-Cowan Connectivity

Furthermore, we examine whether the evolved reservoir recapitulates the signed connectivity structure of the WC model at the population level. The edge polarity across repetitions are shown in Fig. 5 (d), where the percentage of excitatory  $E \rightarrow I$  and inhibitory  $I \rightarrow E$  connections varies and falls below the WC prediction of 100%, the correct sign tendency is present in the majority of repetitions. Panel (e) shows mean shortest path lengths in the  $E \rightarrow I$  and  $I \rightarrow E$  directions, which remain largely symmetric across repetitions, indicating that

the network does not replicate the fast-excitation, delayed-inhibition temporal asymmetry of the WC model at the topological level.

The most direct structural comparison is provided by panel (f). The WC ground truth connectivity matrix (top) has the sign pattern:  $w_{EE} > 0$ ,  $w_{EI} < 0$ ,  $w_{IE} > 0$ ,  $w_{II} = 0$ . The evolved network's mean population connectivity matrix (bottom) recovers the correct sign for three of four interactions:  $E \rightarrow E$  (+0.024),  $E \rightarrow I$  (-0.124), and  $I \rightarrow E$  (+0.073) all match the WC signs. The sole deviation is  $I \rightarrow I$  (-0.139), which deviates from the WC value of zero through stronger lateral inhibition within the I-population. Importantly, this lateral  $I \rightarrow I$  inhibition ( $|\bar{w}| = 0.47 \pm 0.12$ ) is consistently stronger than  $I \rightarrow E$  inhibition ( $|\bar{w}| = 0.31 \pm 0.28$ ) across 9/10 repetitions, constituting a novel emergent inhibitory motif absent in the original WC formulation but consistent with known interneuron physiology in cortical circuits<sup>17</sup>.

These results demonstrate that the PDNE evolution process, driven purely by prediction performance, spontaneously recovers the qualitative E-I connectivity structure of the Wilson-

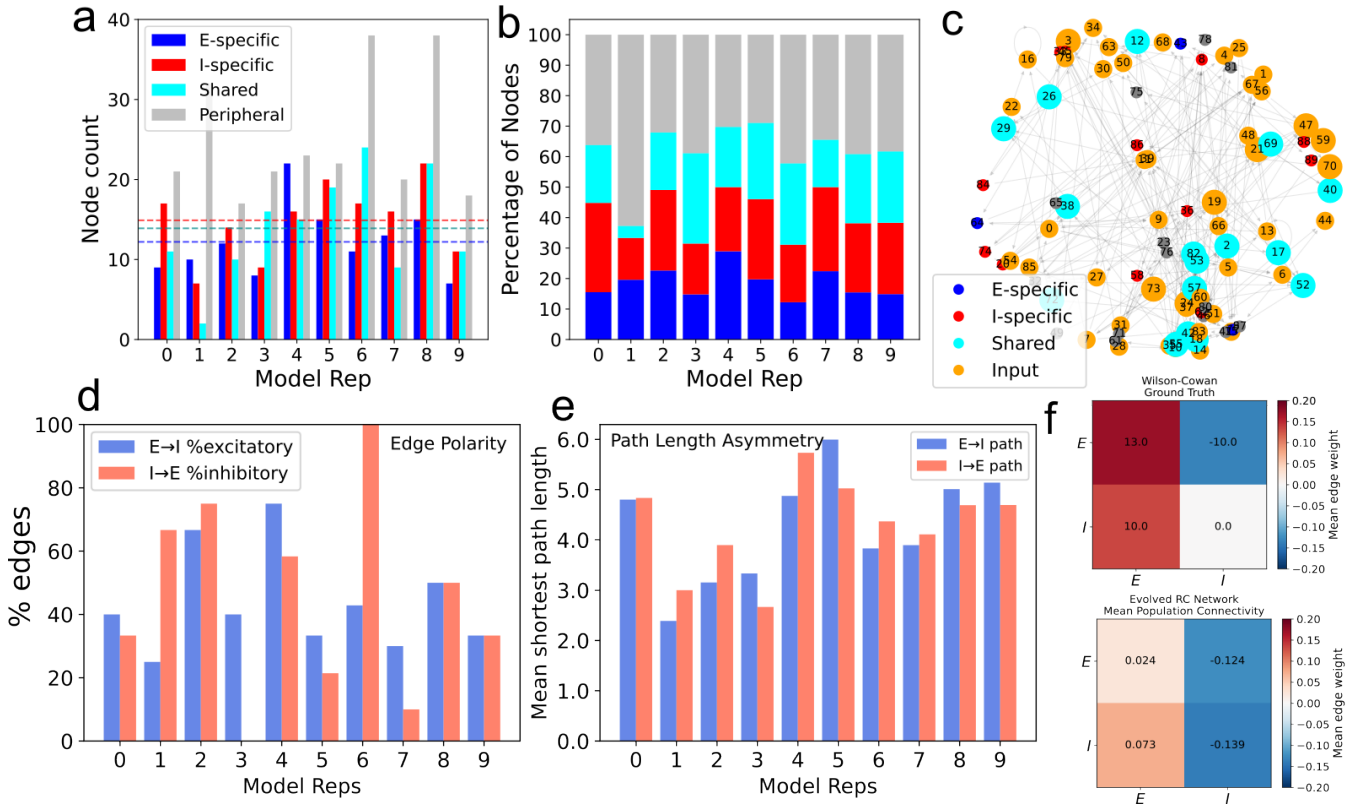


FIG. 5. **Structural analysis of evolved reservoirs and comparison with the Wilson-Cowan E-I architecture.** (a) Node classification counts per repetition: E-specific (blue), I-specific (red), Shared (cyan), Peripheral (gray). Dashed lines: cross-repetition means. (b) Stacked percentage node composition per repetition. (c) Representative evolved network colored by functional role: E-specific (blue), I-specific (red), Shared (cyan), Input (orange). (d) Edge polarity: % of E→I connections that are excitatory (blue) and I→E connections that are inhibitory (red) per repetition. (e) Mean shortest path lengths E→I (blue) and I→E (red) per repetition. (f) WC ground truth connectivity matrix (top) and mean evolved network population connectivity matrix (bottom), showing sign correspondence for three of four E-I interaction types.

Cowan model. The evolved reservoir does not replicate the explicit two-node WC architecture, but instead develops a distributed multi-node solution whose population-level connectivity signs are consistent with the underlying neuronal coupling, providing a structurally interpretable, compact model of E-I physiological rhythms.

## V. DISCUSSION

This study demonstrates that performance-driven network evolution can produce compact, accurate, and structurally interpretable models of neuronal population dynamics. By applying the PDNE framework to the Wilson-Cowan system, we show that reservoirs evolved purely on prediction performance develop internal organizations that spontaneously reflect the E-I architecture of the target neuronal model, without this correspondence being imposed by design.

The prediction results establish that PDNE-evolved reservoirs of  $66 \pm 17$  nodes generalize reliably across unseen stimulus amplitudes and, more strikingly, to entirely novel stimulus configurations varying in pulse number, position, and amplitude without any retraining. This zero-shot generalization

indicates that the evolved networks have internalized the reactive dynamics of the WC system, its stimulus-driven transient responses, timescale separation between E and I populations, and recovery between successive pulses rather than memorizing specific training patterns. This has direct implications for data-efficient digital twinning of neuronal systems, where training data may be limited to a narrow range of experimental conditions.

The structural analysis reveals two complementary findings. First, the functional node composition approximately equal proportions of E-specific, I-specific, and shared nodes, consistent across stochastically distinct repetitions, which demonstrates that PDNE evolution reliably organizes the reservoir into populations mirroring the E-I structure of the target system. The consistency of this organization across networks of varying size suggests it reflects a fundamental property of the task rather than a particular network instantiation. Second, the population-level connectivity of the evolved networks spontaneously recovers the correct excitatory–inhibitory sign pattern of the WC model for three of four interaction types. The sole structural deviation, stronger lateral I→I inhibition relative to I→E inhibition constitutes a novel emergent motif that is absent in the original

WC formulation but is well-known in cortical interneuron physiology<sup>17</sup>. This suggests that the evolution process discovers a broader class of E-I stabilization mechanisms beyond those encoded in the target model, potentially revealing alternative dynamical solutions that are biologically plausible.

These findings have several broader implications. For neuronal modeling, they demonstrate that structure-function relationships in E-I networks can be recovered from dynamics alone, without anatomical constraints or explicit supervision of connectivity. For reservoir computing, they establish that PDNE provides a principled path from uninformative random reservoirs to task-adapted, structurally interpretable networks. For RC-based digital twin construction<sup>18</sup>, they suggest that compact evolved reservoirs can serve as mechanistically transparent surrogates for neuronal systems, capturing not only the output dynamics but also the organizational principles of the underlying circuit.

Several directions merit future investigation. Extending the framework to more complex neuronal models: multi-population networks, spatially structured cortical circuits, or models exhibiting sustained oscillations and chaos will test the generality of the structural correspondence finding. Incorporating biophysical constraints on network connectivity during evolution (e.g., Dale’s principle separating excitatory and inhibitory neurons) may further sharpen the structural interpretability of the evolved reservoirs. Finally, applying PDNE to experimental neural time-series data, where the ground truth connectivity is unknown, represents the ultimate test of whether performance-driven evolution can serve as a tool for circuit inference from dynamics.

By bridging insights from network science, reservoir computing, and computational neuroscience, this work opens new avenues for building efficient, interpretable, and structurally meaningful models of physiological rhythms, a step toward compact digital twins of neuronal systems grounded in dynamical first principles.

## DATA AVAILABILITY STATEMENT

All Python codes for numerical simulations and data generated in this study are publicly available at: [github.com/maneesh51/PDNE-WilsonCowanNeuron](https://github.com/maneesh51/PDNE-WilsonCowanNeuron) <https://github.com/maneesh51/PDNE-WilsonCowanNeuron>

## Appendix A: Model Parameters

### Wilson–Cowan Neuron Model

Parameters for the WC model (Eqs. (2)–(4)):  $\tau_E = 10$ ,  $\tau_I = 5$ ,  $w_{EE} = 13$ ,  $w_{EI} = 10$ ,  $w_{IE} = 10$ ,  $w_{II} = 0$ ,  $a_E = 6$ ,  $a_I = 4$ ,  $\theta_E = 2.5$ ,  $\theta_I = 2.0$ . The external pulse stimulus is:

$$s(t) = \begin{cases} S_{\text{amp}}, & 20 < t < 80 \\ 0, & \text{otherwise} \end{cases} \quad (\text{A1})$$

with training amplitudes  $\mathcal{A}_{\text{train}} = \{1.25, 1.5, 2.0, 2.5, 3.0\}$  and test amplitudes  $\mathcal{A}_{\text{test}} = \{0.85, 1.4, 1.75, 2.25, 2.75\}$ . The system is integrated using `solve_ivp` with a time span of  $T_{\text{max}} = 175$  s, integration step  $\delta t = 0.1$  s, and subsampled by a factor of 10 to obtain the RC input-output sequences of length  $N_{\text{pts}} = 3000$  per trial.

### Initial seed Network

The initial seed network is a random directed Erdős–Rényi network of  $N_0 = 25$  nodes with mean degree  $K_S = 1$  and initial spectral radius  $\rho_0 = 0.2$ . Input and output node sets  $\mathcal{I}$  and  $\mathcal{O}_{E,I}$  are initialized by randomly selecting  $\lfloor P_{\text{inp}} \cdot N_0 \rfloor$  and  $\lfloor P_{\text{out}} \cdot N_0 \rfloor$  nodes respectively. Node gain values are drawn uniformly:  $g_i \sim \mathcal{U}(0.01, 1.0)$ .

### PDNE and RC Hyperparameters

All hyperparameters are fixed across all 10 model repetitions and summarized in Table I.

TABLE I. PDNE and RC hyperparameters.

Parameter	Symbol	Value
<i>Reservoir Computing</i>		
Leak rate	$\alpha$	0.2
Spectral radius	$\rho$	0.2
Ridge parameter	$\beta$	$5 \times 10^{-10}$
Transient steps	$T_{\text{trans}}$	10
RC repetitions	$N_{\text{RC}}$	1
Number of inputs	$N_I$	1
Number of outputs	$N_O$	2
<i>Network Evolution</i>		
Max evolution steps	$T$	200
Target NMSE	$\Delta_{\epsilon}$	0.005
Error precision	–	6 digits
Max addition attempts	$T_{\text{add}}$	25
Max new links	$k_{\text{max}}$	5
Connection probability	$\Psi$	0.5
Input node probability	$P_{\text{inp}}$	0.5
Output node probability	$P_{\text{out}}$	0.5
Node gain range	$g \sim \mathcal{U}$	(0.01, 1.0)
Deletion percentage	$p_{\text{del}}$	20%
Input node type	–	Non-exclusive (0)
Output node type	–	Non-exclusive (0)
<i>Seed Network</i>		
Number of nodes	$N_0$	25
Mean degree	$K_S$	1
Initial spectral radius	$\rho_0$	0.2

<sup>1</sup>G. Buzsáki and A. Draguhn, “Neuronal oscillations in cortical networks,” *Science* **304**, 1926–1929 (2004).

<sup>2</sup>X.-J. Wang, “Neurophysiological and computational principles of cortical rhythms in cognition,” *Physiological Reviews* **90**, 1195–1268 (2010).

<sup>3</sup>O. Sporns, *Networks of the Brain* (MIT Press, Cambridge, MA, 2011).

<sup>4</sup>C. Rudin, “Stop explaining black box machine learning models for high stakes decisions and use interpretable models instead,” *Nature Machine Intelligence* **1**, 206–215 (2019).

- <sup>5</sup>H. R. Wilson and J. D. Cowan, “Excitatory and inhibitory interactions in localized populations of model neurons,” *Biophysical Journal* **12**, 1–24 (1972).
- <sup>6</sup>C. Rackauckas, Y. Ma, J. Martensen, C. Warner, K. Zubov, R. Sipekar, D. Skinner, A. Ramadhan, and A. Edelman, “Universal differential equations for scientific machine learning,” arXiv preprint (2020), arXiv:2001.04385.
- <sup>7</sup>D. Durstewitz, G. Koppe, and M. I. Thurm, “Reconstructing computational dynamics from neural measurements with recurrent neural networks,” *Nature Reviews Neuroscience* **24**, 693–710 (2023).
- <sup>8</sup>H. Jaeger, “The “echo state” approach to analysing and training recurrent neural networks,” *GMD Report* **148** (2001), German National Research Center for Information Technology.
- <sup>9</sup>W. Maass, T. Natschläger, and H. Markram, “Real-time computing without stable states: A new framework for neural computation based on perturbations,” *Neural Computation* **14**, 2531–2560 (2002).
- <sup>10</sup>D. Verstraeten, B. Schrauwen, M. d’Haene, and D. Stroobandt, “An experimental unification of reservoir computing methods,” *Neural Networks* **20**, 391–403 (2007).
- <sup>11</sup>C. Gallicchio, A. Micheli, and L. Pedrelli, “Deep reservoir computing: A critical experimental analysis,” *Neurocomputing* **268**, 87–99 (2017).
- <sup>12</sup>M. Lukoševičius, “A practical guide to applying echo state networks,” in *Neural Networks: Tricks of the Trade*, edited by G. Montavon, G. B. Orr, and K.-R. Müller (Springer, Berlin, Heidelberg, 2012) pp. 659–686.
- <sup>13</sup>B. Schrauwen, M. Wardermann, D. Verstraeten, J. J. Steil, and D. Stroobandt, “Improving reservoirs using intrinsic plasticity,” in *Neurocomputing*, Vol. 71 (2008) pp. 1159–1171.
- <sup>14</sup>M. Yadav, S. Sinha, and M. Stender, “Evolution beats random chance: Performance-dependent network evolution for enhanced computational capacity,” *Physical Review E* **111**, 014320 (2025).
- <sup>15</sup>A. Radhakrishnan, J. F. Lindner, S. T. Miller, S. Sinha, and W. L. Ditto, “Growing neural networks: dynamic evolution through gradient descent,” *Proceedings of the Royal Society A* **481**, 20250222 (2025).
- <sup>16</sup>M. Yadav and M. Stender, “Task-specific node pruning enhances computational efficiency of reservoir computing networks,” *Chaos: An Interdisciplinary Journal of Nonlinear Science* **35**, 083123 (2025).
- <sup>17</sup>R. Tremblay, S. Lee, and B. Rudy, “GABAergic interneurons in the neocortex: From cellular properties to circuits,” *Neuron* **91**, 260–292 (2016).
- <sup>18</sup>M. Yadav, S. Chauhan, M. D. Shrimali, and M. Stender, “Predicting multi-parametric dynamics of an externally forced oscillator using reservoir computing and minimal data,” *Nonlinear Dynamics* (2024), 10.1007/s11071-024-10720-w.